Supporting Information

Three-dimensional covalent organic framework based artificial interphase layer endowed the highly stable lithium metal anode

Kaiyang Zheng,[a] Zhengyang Gou,[a] Cen Zhang,[a] Yuqiang Zhang,[a] Yaying Dou,[bc] Shaojie Liu,[a] Yongheng Zhang,[d] Yantao Zhang*[a]*

[a] College of Chemistry and Pharmaceutical Engineering, Hebei University of Science and Technology, Shijiazhuang, 050018, China. E-mail: sjliu16@163.com; ytzhang@hebust.edu.cn

[b] Interdisciplinary Research Center for Sustainable Energy Science and Engineering (IRC4SE^2), School of Chemical Engineering, Zhengzhou University, Zhengzhou 450001, China.

[c] Key Laboratory of Advanced Energy Materials Chemistry (Ministry of Education), College of Chemistry, Nankai University, Tianjin 300071, China.

[d] Risun New Energy Technology Co., Ltd. Beijing 100070, China.

1. Materials

The 4-[tris(4-aminophenyl)methyl]aniline (TAPM) was purchased from Shanghai Haohong Scientific Co., Ltd.2,5-Dihydroxyterephthalaldehyde (DHBA) was purchased from Jiangsu Aikang Biopharmaceutical Co., Ltd. Glacial acetic acid was purchased from Shanghai MacLean Biochemical Co., Ltd. N, N-dimethylacetamide (DMAc), o-dichlorobenzene (o-DCB), N-methyl-2-pyrrolidone (NMP), tetrahydrofuran (THF), and acetone were supplied by Shanghai Aladdin Biochemical Technology Co., Ltd. 1 M LiTFSI in 1,3-dioxane (DOL)/1,2-dimethoxyethane (DME) electrolyte (volume ratio 1:1) with 2 wt% $LiNO_3$, and the carbonate electrolyte of 1M $LiPF_6$ in ethylene carbonate (EC)/dimethyl carbonate (DMC)/ethyl methyl carbonate (EMC) (volume ratio 1:1:1) were purchased from DoDochem Technology Co., Ltd. CR2032 coin-type cells, polyvinylidene fluoride (PVDF), polypropylene (PP) separators, lithium metal foil, copper foil, aluminum foil were purchased from Guangdong Canrd New Energy Technology Co., Ltd.

2. Synthesis of TD-COF

TD-COF was synthesized according to previous literature. [1] TAPM (25.4 mg) and DHBA (22.1 mg) were placed in a Pyrex tube with N, N-dimethylacetamide (DMAc) and o-dichlorobenzene (o-DCB) as solvents and acetic acid as catalyst. The obtained mixture was sonicated for 30 min after the addition of acetic acid (6 M, 0.35 mL) and then heat-sealed after subjected to three cycles of vacuum degassing at 77 K in a liquid nitrogen bath. After reaction at 120 ℃ for three days, the compounds were collected after centrifugation, washed with THF and dried in sequence. Further, the dried product was extracted by Soxhlet in THF for one day, and then washed with acetone. Finally, the orange powder identified as TD-COF was collected after vacuum drying at 70 ℃ overnight.

3. Preparation of LiTFSI@TD-COF

100 mg LiTFSI was dissolved in ethanol (10 mL), and then TD-COF (100 mg) was added to the above solution. After stirring for 24 hours at room temperature, the mixture was filtered, and LiTFSI@TD-COF powder was obtained after vacuum drying

at 120 ℃ for 12 h.

4. Material characterizations

The chemical composition and elements of the samples were analyzed using Fourier transform infrared (FT-IR) spectra (Thermo Fisher Scientific, Nicolet iS5), Raman spectra (LabRAM HR 800), and X-ray photoelectron spectroscopy (XPS, ESCALAB 250XI, Mg-Kα radiation). The ^{7}Li and ^{13}C solid-state NMR measurements of the samples were conducted on Bruker AVANCE III 500 spectrometer. ^{7}Li solid-state NMR spectra sample were used with a 3.2 mm probe head under spinning frequency of 10 kHz. The repetition times of 10 s were set and a π/4 pulse length were utilized for ^{7}Li acquisition to ensure the complete relaxation. X-ray diffraction (XRD, Rigaku D/MAX-2500) was used to obtain the crystal structure of the material, using a Cu Kα source (λ = 1.5406 Å) in the range of 2θ = 2.0 ~ 50.0°. The Rietveld refinement of crystal structure and the simulated structure of TD-COF were performed with Materials Studio software. N_2 adsorption and desorption isotherms were collected by Autosorb iQ-Quantachrome Instrument at 77 K. Prior to adsorption measurement, the powder was degassed at 150 °C for more than 12 hours. The specific surface area was calculated according to the Brunauer-Emmett-Teller (BET) method, and pore size distributions were derived on the basic of nonlocal density functional theory (NLDFT) model. Scanning electron microscope (SEM, Hitachi S-4800) and high-resolution transmission electron microscope (HRTEM, JEOL, JEM-2100) were used to observe the micro-morphology of the samples.

5. Preparation of electrodes

TD-COF@Cu electrode: TD-COF and PVDF were mixed in a mass ratio of 9:1, and an appropriate amount of anhydrous NMP was added and mixed uniformly. The well-mixed slurry was then coated onto Cu foil (Φ = 12 mm) and vacuum dried overnight at 60 ℃.

TD-COF@Li electrode: To fabricate 1 wt% TD-COF@NMP suspension solution, 10 mg of TD-COF powder was blended with 990 mg of anhydrous NMP after 30 min ultrasonic dispersion. 50μL of 20 mg mL^{-1} PVDF@NMP solution was added into the

above suspension. 40 μL of the mixed solution was evenly dripped onto a Li foil (Φ = 16 mm). Subsequently, the TD-COF coated Li foil was vacuum-dried in glove box chamber, and TD-COF@Li electrode was punched into 10 mm-diameter Li disk.

$LiFePO_4$ cathode: The mixture sulfur containing $LiFePO_4$ (LFP) powder, Super P carbon and PVDF (8:1:1 in weight) dissolved in appropriate amount of anhydrous NMP was uniformly scrape-coated onto aluminum (Al) foil with a diameter of 12mm. The obtained Al foils were dried overnight at 80 ℃ in vacuum. The active material loading on each Al foils is approximately 2.9 mg.

Sulfur cathode: KB@S composite was prepared by grinding sulfur powder (S) and Ketjen black in a mass ratio of 7:3 and heating at 150 ℃ for 12 hours. KB@S, Super Li, and PVDF (8:1:1 in weight) were mixed in NMP solution to form a uniform slurry. The well-mixed slurry was coated onto Al foil (Φ = 12 mm), and vacuum-dried overnight at 60 ℃. The active material loading on each Al foil is approximately 1.6 mg.

6. Cells assembly and electrochemical tests

CR2032 coin-type cells were assembled in an argon-filled glove box (Etelux Lab 2000) with O_2 and H_2O levels < 0.1 ppm. The electrochemical performances were tested on LAND battery instruments (CT3002A) at constant temperature of 25℃.

Li|Cu half cell: The asymmetric Li|Cu cells were fabricated with bare Cu or TD-COF@Cu as the working electrode and pristine lithium foil as the counter electrode separated with Celguard 2400 microporous film soaked in 45μL 1 M LiTFSI in DOL/DME with 2 wt% $LiNO_3$ electrolyte. The voltage-time profiles were recorded at different current densities of 0.5 mA cm^{-2}, 1 mA cm^{-2} and 2 mA cm^{-2} with the deposition capacity limit of 1 mAh cm^{-2} at the cut-off voltage of 1.7 V (vs. Li/Li^+).

Li|Li symmetric cell: The symmetric cells consisted of bare Li or TD-COF@Li as both sides of electrodes separated from PP membrane by 40μL 1 M LiTFSI electrolyte in DOL/DME with 2 wt% $LiNO_3$ electrolyte. The charge and discharge tests were performed at different current densities of 5, 10, 20 mA cm^{-2} with the he same fixed deposition capacity of 5 mAh cm^{-2}. Rate performance was carried out at 1 mAh cm^{-2} deposition capacity with different current densities of 0.25, 0.5, 1.0, 2.0, 4.0, and 6.0

mA cm^{-2}.

Li|LFP full cell: The as-prepared LFP electrodes and bare Li or TD-COF@Li used as cathode and anode electrodes respectively, were stacked together with a sandwiched PP separator immersed in 40μL 1.0 M $LiPF_6$ EC/DMC/EMC electrolyte. The galvanostatic charge and discharge curves and rate performance were collected between the voltage range of 2.5-3.75 V (vs. Li/Li^+) at different current densities (1C=170 mA g^{-1}).

Li|S full cell: The Li|S full cell was configured with the as-prepared KB@S cathode and bare Li or TD-COF@Li anode electrodes and a Celguard 2400 separators impregnated in 40μL 1 M LiTFSI in DOL/DME with 2 wt% $LiNO_3$ electrolyte. The galvanostatic charge and discharge test and rate performance were recorded between the voltage range of 1.7-2.8 V (vs. Li/Li^+) at different current densities of 0.1, 0.2, 0.5, 1.0 and 1.5C. (1C=1675 mA g^{-1}).

In situ cell: Primarily, bare Li or TD-COF@Li were sheared into squares with 10 mm sides, and assembled into the home-made in-situ optical cell filled with 1 mL of 1 M LiTFSI in DOL/DME with 2 wt% $LiNO_3$ electrolyte. Subsequently, the cells were tested on Neware battery test system, and the process of lithium dendrites growth was observed by optical microscopy (ZEISS Stemi 508) at a current density of 5 mA cm^{-2}.

7. Electrochemical impedance spectroscopy (EIS) test

Electrochemical impedance spectra (EIS) were performed on electrochemical workstation (Bio-logic VSR-300, FR) with 5 mV fluctuations in the frequency range from 100 kHz to 10 mHz. The corresponding fitting equivalent circuit model and parameters are shown in Supporting Information.

8. Li^+ transference number (t_{Li^+}) test

The Li^+ transfer number (t_{Li^+}) was tested based on the Li|Li symmetric cell, and calculated by a combination of direct current (DC) polarization and alternating current (AC) impedance. The Li^+ transfer number can be calculated using the Bruce-Vincent formula as follows. [2,3]

$$t_{Li+} = \frac{I_{ss}R_{eSS}(\Delta V - I_0R_0)}{I_0R_{e0}(\Delta V - I_{SS}R_{SS})}$$

where ΔV is the polarization potential of potentiostatic DC polarization. I_0 and I_{SS}, R_e^0 and R_e^{SS}, R_0 and R_{SS} are the current values, electrolyte resistance, and interphase resistance of initial and steady state respectively, before and after DC polarization.

Theoretical calculations

The interplay of lithium bis(trifluoromethanesulfonyl)imide (LiTFSI) molecules with electrolyte solvent and TD-COF fragments were analyzed via calculating the adsorption energy using Gaussian 09 software package. During geometry and frequency optimization, all systems were relaxed. Based on density functional theory (DFT), quantum cluster calculations were performed in THF environment using the B3LYP function and the 6-31G$^+$(d, p) basis set with the SMD solvation model set (ε = 7.4257). Taking TD-COF and Li^+ as an example, the formula for adsorption energy calculation is as follows:

$$E_{abs} = E_{Li+TD-COF} - E_{TD-COF} - E_{Li}$$

Where $E_{Li+TD-COF}$, E_{TD-COF}, and E_{Li} represent the optimized energy of TD-COF fragment adsorbing Li^+, TD-COF fragment, and isolated Li atom, respectively.

The simulated calculations for the possible Li^+ migration pathways through TD-COF were carried out using the DMol3 software in the Materials Studio package. The LST/QST method was used to search for transition states, and the generalized gradient approximation (GGA), Perdew-Burke (PBE) functional, and DFT Semi-core Pseudopots (DSPP) were used to handle theoretical energy barriers. Similarly, DMol3 software was also used to calculate Mulliken population analysis and electrostatic potential distribution in B3LYP functional and DND basis set.

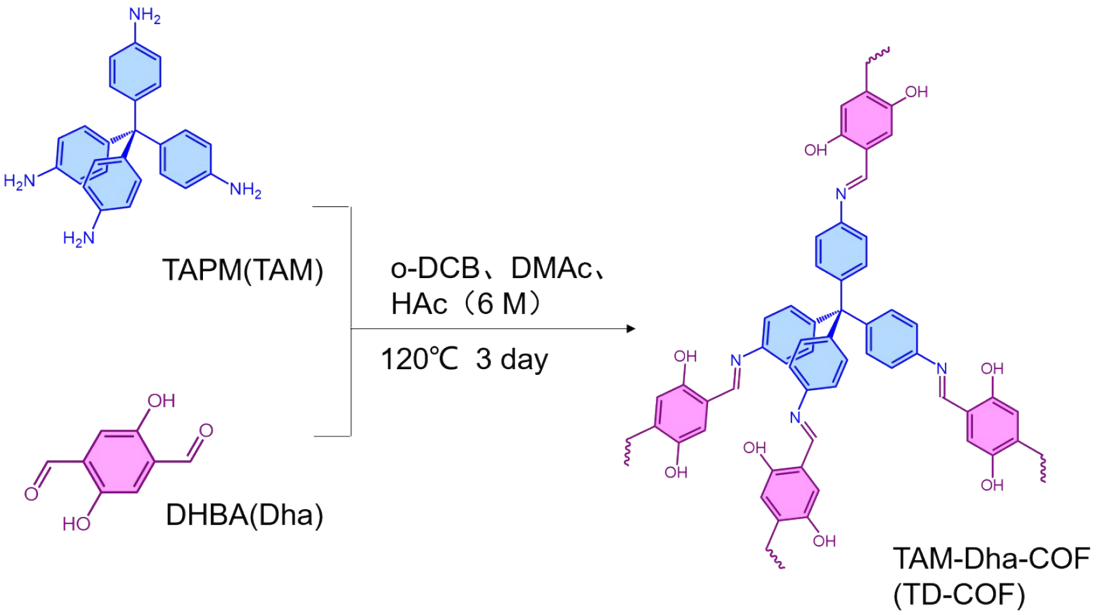

Fig. S1. Synthetic processes of TD-COF.

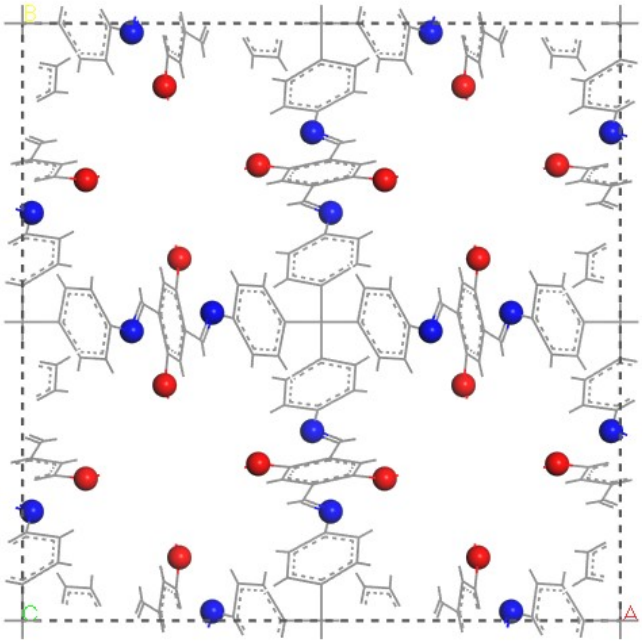

Fig. S2. Unit cell structures of TD-COF.

Table S1. Calculated unit cell parameters and fractional atomic coordinates based on 7-fold interpenetrated TD-COF.

Space group symmetry	**I 41/a (No.88)**		
Calculated unit cell	**a = b = 19.81 Å, c = 9.08 Å, α = γ = β = 90°**		
Atoms	**x**	**y**	**z**
C7	0.09690	0.44050	1.10958
C4	0.11464	0.55434	0.93240
N1	0.18264	0.48455	0.75876
C2	0.06098	0.49999	1.14383
C3	0.7195	0.55710	1.05426
C6	0.13941	0.43770	0.98714
C5	0.14747	0.49377	0.89555
C10	0.26371	0.43377	0.33269
C8	0.20024	0.53129	0.66623
C9	0.22824	0.51400	0.51996
C11	0.24310	0.44798	0.47754
H6	0.16396	0.39453	0.95951
H7	0.08915	0.39453	1.17082
H4	0.11814	0.59860	0.86370
H3	0.04384	0.60295	1.07397
H8	0.19171	0.58394	0.69108
H11	0.23766	0.39422	0.57900
H10	0.27503	0.38228	0.30094
H	0.24975	0.34832	0.53733
C1	0.00000	0.50000	1.25000

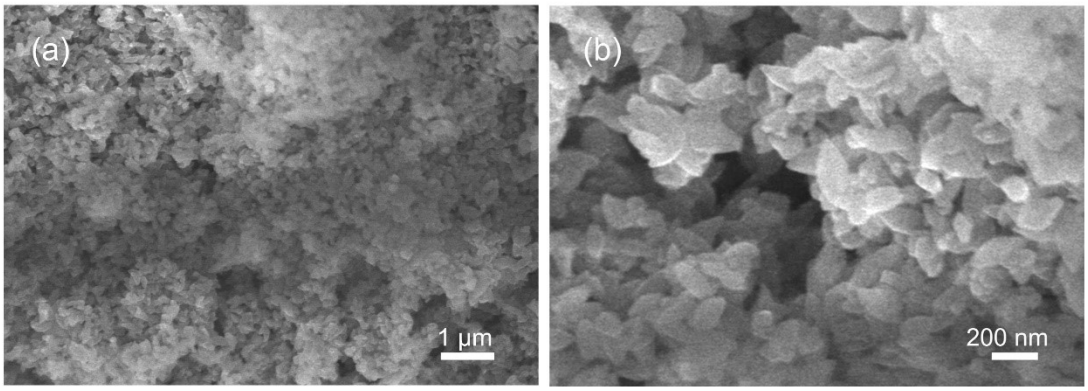

Fig. S3. SEM images of TD-COF.

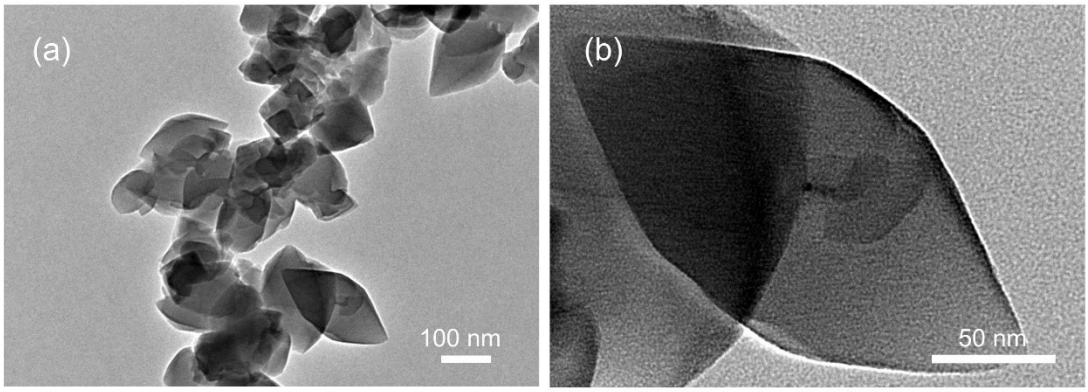

Fig. S4. HRTEM images of TD-COF.

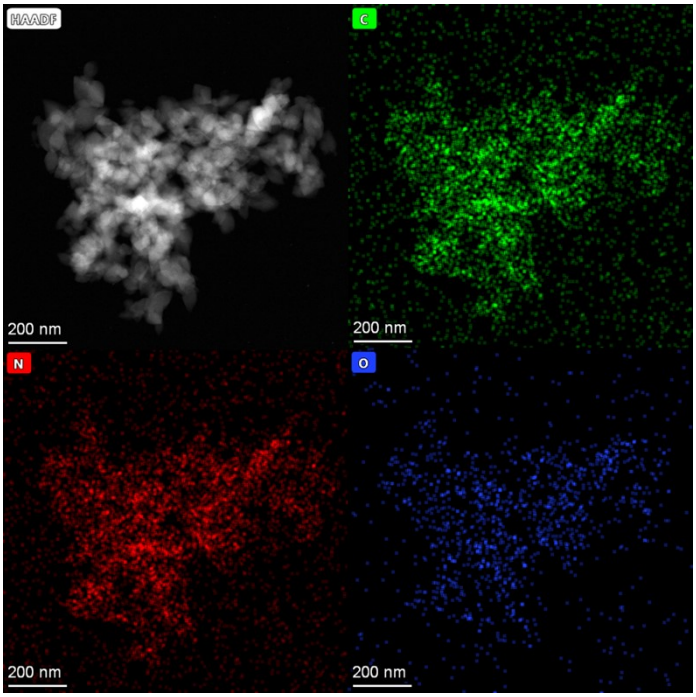

Fig. S5. EDS spectra of TD-COF.

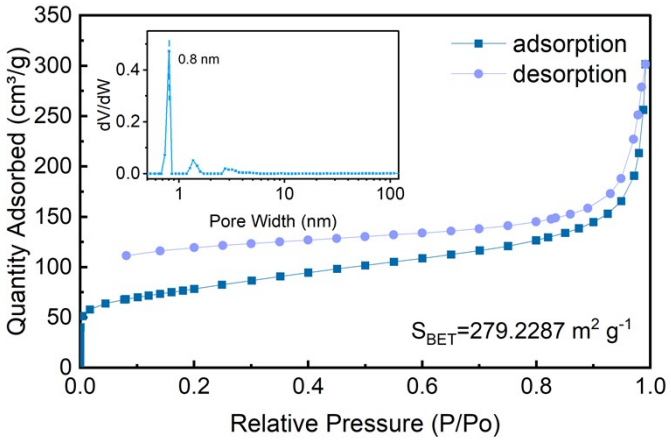

Fig. S6. N_2 adsorption and desorption isotherms and corresponding pore size distribution.

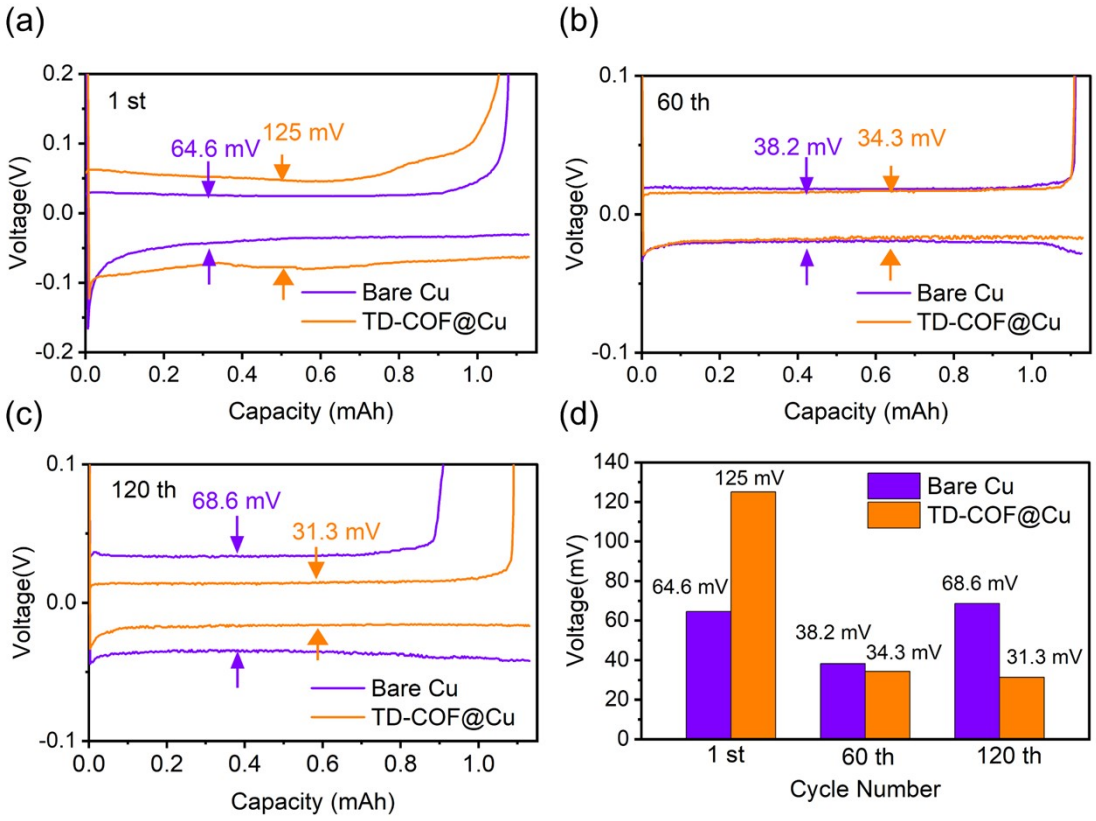

Fig. S7. The comparisons of voltage hysteresis (a-c) and polarization (d) of Li|Cu cells with and without TD-COF@Cu electrode operated at 0.5 mA cm^{-2} with 1 mAh cm^{-2}.

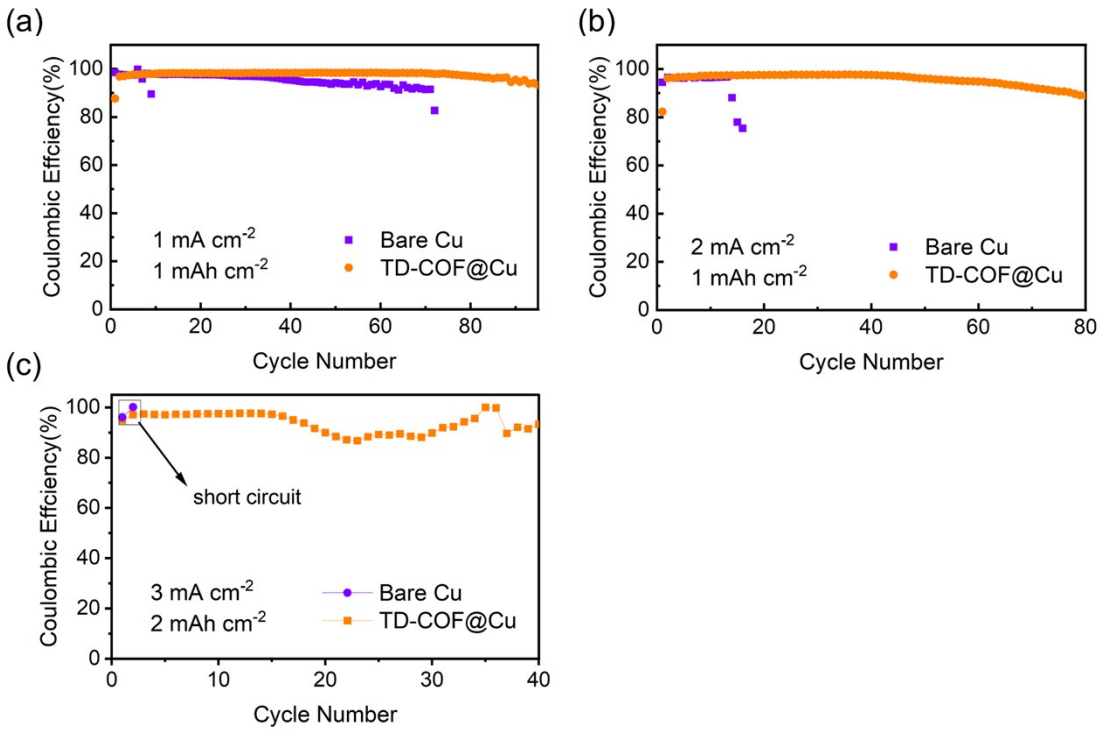

Fig. S8. The Coulombic efficiency of Li|Cu cells with and without TD-COF modified Li metal anodes operated at different current densities.

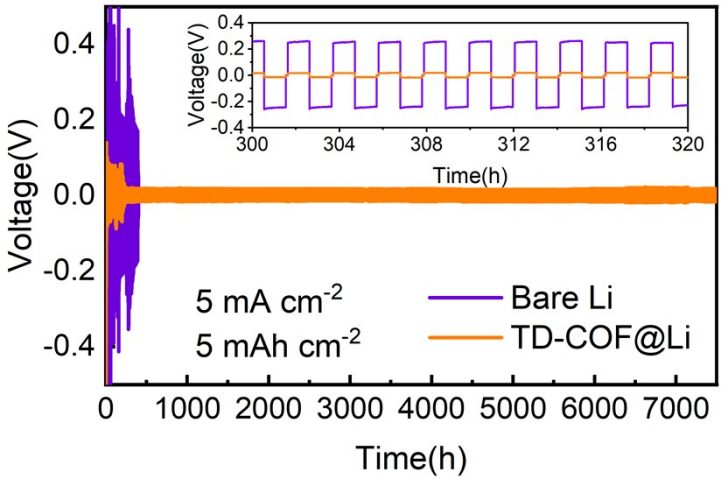

Fig. S9. Long cycle performance of Li|Li symmetric batteries operated at current density of 5mA cm^{-2} with fixed capacity of 5mA cm^{-2}.

Table S2. The comparison of Li|Li symmetric batteries modified with different materials.

Modifications	Coating methode	Over potential (mV)	Current/Capacity Density	Electrolyte	Cycling time (h)	References
TpTt coated separators	Slurry casting	14	1.0 mA cm^{-2} 2.0 mA h cm^{-2}	1 M LiTFSI in DOL/DME (v/v= 1/1) with 2 wt.% $LiNO_3$	1000	4
TpPa-COF-protected lithium anodes	In-situ prepared on the Li foil	80	10.0 mA cm^{-2} 5.0 mA h cm^{-2}	1 M LiTFSI in DOL/DME (v/v= 1/1) with 1 wt.% $LiNO_3$	200	5
COF-LZU1 coated Li anode as Artificial SEI	Suspension dropping	35	0.5 mA cm^{-2} 0.5 mA h cm^{-2}	1 M LiTFSI in DOL/DME (v/v= 1/1) with 1 wt.% $LiNO_3$	2000	6
NO_2-COF coated Li anode as Artificial SEI	Suspension dropping	20.7	10 mA cm^{-2} 10 mA h cm^{-2}	1 M LiTFSI in DOL/DME (v/v= 1/1) with 1 wt.%	1000	7
COF-LZU1 coated separators	Suspension dropping	50	1 mA cm^{-2} 1 mA h cm^{-2}	1 M LiTFSI in DOL/DME (v/v= 1/1) with 1 wt.% $LiNO_3$	1000	8
Co-spc-COP coated Li anode as Artificial SEI	Suspension dropping	42 115 98	2 mA cm^{-2} 2 mA h cm^{-2} 3 mA cm^{-2} 1 mA h cm^{-2} 5 mA cm^{-2} 1 mA h cm^{-2}	1 M LiTFSI and 0.2 M $LiNO_3$ in DOL/DME (v/v= 1:1)	3400 6600 1600	9

Highly nitrogen-rich COF protection layers	In-situ prepared on the Li foil	80 118.8	5.0 mA cm^{-2} 5.0 mA h cm^{-2} 20 mA cm^{-2} 20 mA h cm^{-2}	1 M LiTFSI in DOL/ DME (v/v= 1/1) with 2 wt.% $LiNO_3$	8000 1600	10
sp^2c-COF-Co coated Li anode as Artificial SEI	Suspension dropping	16 20 24	2 mA cm^{-2} 2 mA h cm^{-2} 5 mA cm^{-2} 5 mA h cm^{-2} 10 mA cm^{-2} 10 mA h cm^{-2}	1 M LiTFSI in DOL/ DME (v/v= 1/1)	6000 4000 2000	11
HAHATN-PMDA-COF coated Li anode as Artificial SEI	Slurry casting	30	0.5 mA cm^{-2} 1 mA h cm^{-2}	1 M LiTFSI in DOL/ DME (v/v= 8/2) with 10 vol% FEC	600	12
COF-F_6 coated Li anode as Artificial SEI	Suspension dropping	14.2 22	2 mA cm^{-2} 2 mA h cm^{-2} 4 mA cm^{-2} 4 mA h cm^{-2} 5 mA cm^{-2} 5 mA h cm^{-2}	1 M LiTFSI in DOL/ DME (v/v= 1/1)	5500 5000	13
TD-COF coated Li anode as Artificial SEI	Suspension dropping	35.2 46.8 80.8	5.0 mA cm^{-2} 5.0 mA h cm^{-2} 10.0 mA cm^{-2} 5.0 mA h cm^{-2} 20.0 mA cm^{-2} 5.0 mA h cm^{-2}	1 M LiTFSI in DOL/ DME (v/v= 1/1) with 1 wt.% $LiNO_3$	7485 9160 3380	This work

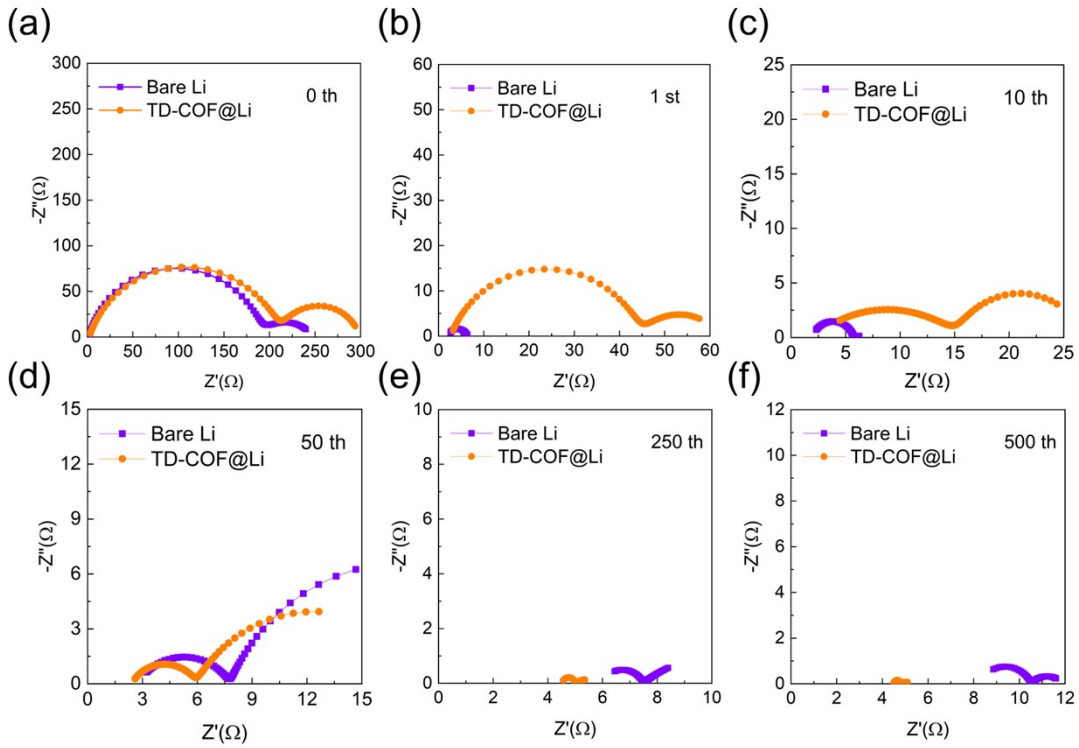

Fig. S10. The plotted EIS of Li|Li symmetric cells with and without the TD-COF layer recorded at different cycle number under current density of 4 mA cm^{-2} with a fixed capacity of 2 mAh cm^{-2}.

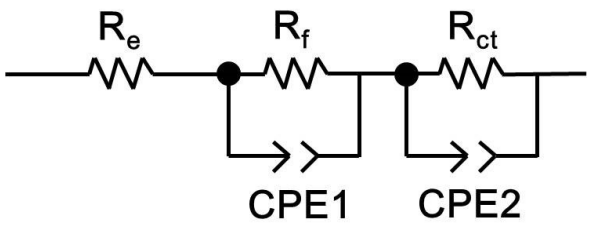

Fig. S11. The equivalent circuit for modeling the Nyquist plots.

Table S3. The calculated impedance parameters derived from Nyquist diagram in **Fig. S10** based on the equivalent circuit model in **Fig. S11**.

Bare Li						
	0 th	1 st	10 th	50 th	250 th	500th
$R_e(\Omega)$	1.794	2.392	1.962	2.744	5.948	8.233
$R_f(\Omega)$	56.79	1.42	0.7226	5.042	1.537	1.397
$R_{ct}(\Omega)$	189.2	2.572	3.752	19.66	5.344	2.276
TD-COF@Li						
	0 th	1 st	10 th	50 th	250 th	500th
$R_e(\Omega)$	1.993	2.681	2.061	2.418	4.511	4.487
$R_f(\Omega)$	86.76	17.7	9.979	3.52	0.4826	0.531
$R_{ct}(\Omega)$	210.5	41.96	13.52	13	0.8888	0.3222

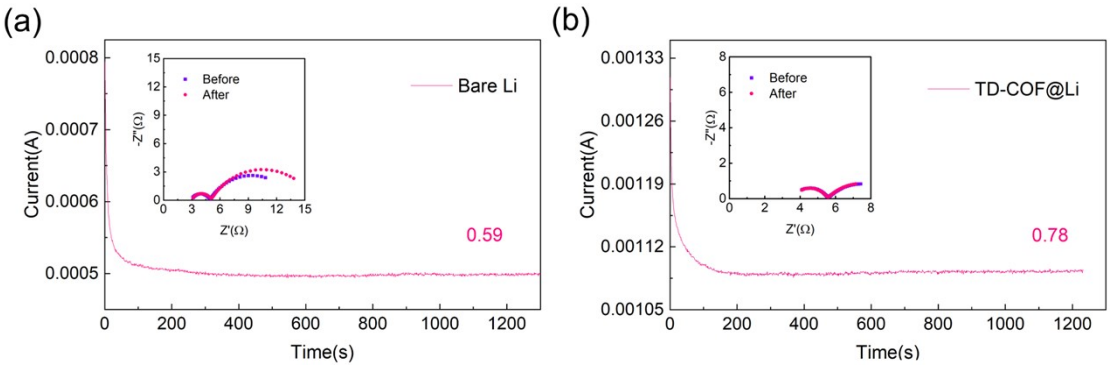

Fig. S12. The constant potential DC polarisation and AC impedance spectra of Li|Li symmetric cells without (a) and with (b) TD-COF after 250 cycles at 4mA cm^{-2} and 2mAh cm^{-2}.

Table S4. The Li^+ transfer number and electrochemical parameters were calculated from constant potential DC polarization and AC impedance spectra.

	I_0(mA)	I_{ss}(mA)	R_0(Ω)	R_{ss}(Ω)	R_e^0(Ω)	R_e^{SS}(Ω)	ΔV(mV)	t_{Li+}
Bare Li	0.794	0.498	2.011	2.07	2.954	2.993	10	**0.595**
TD Li	1.31	1.09	2.013	2.019	3.54	3.535	10	**0.784**

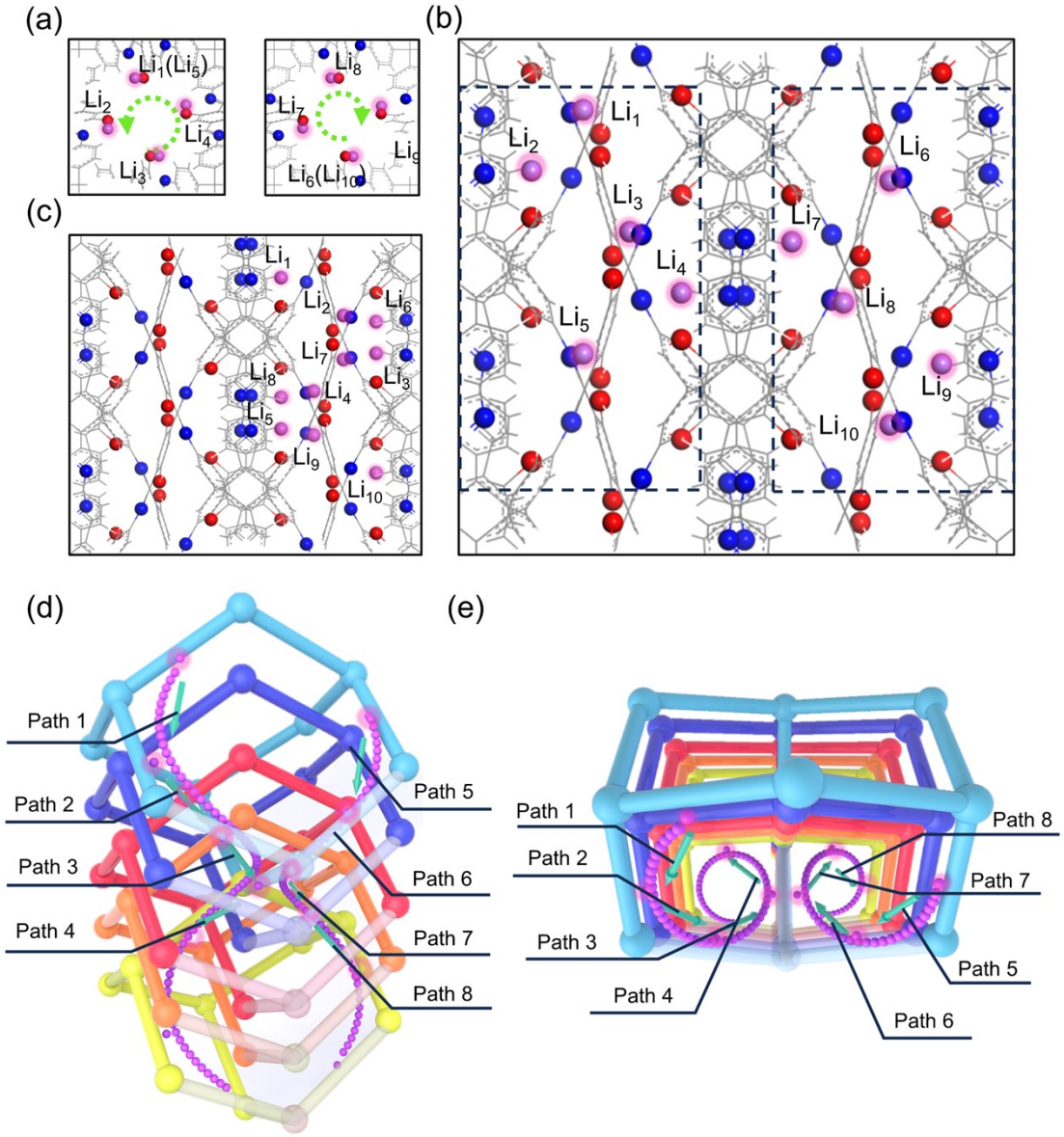

Fig. S13. Three views of migration sites for two migration pathways of Li^+ in TD-COF, top view (a), front view (b), side view (c) and Li^+ migration pathways in TD-COF pores (d and e).

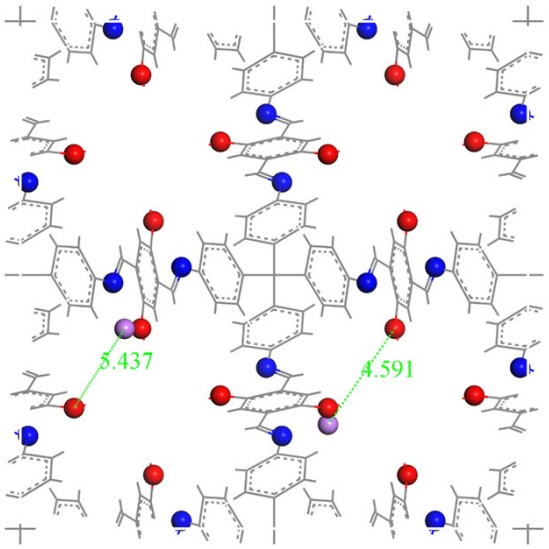

Fig. S14. The contact distance between Li^+ and O atoms in a one-dimensional channel.

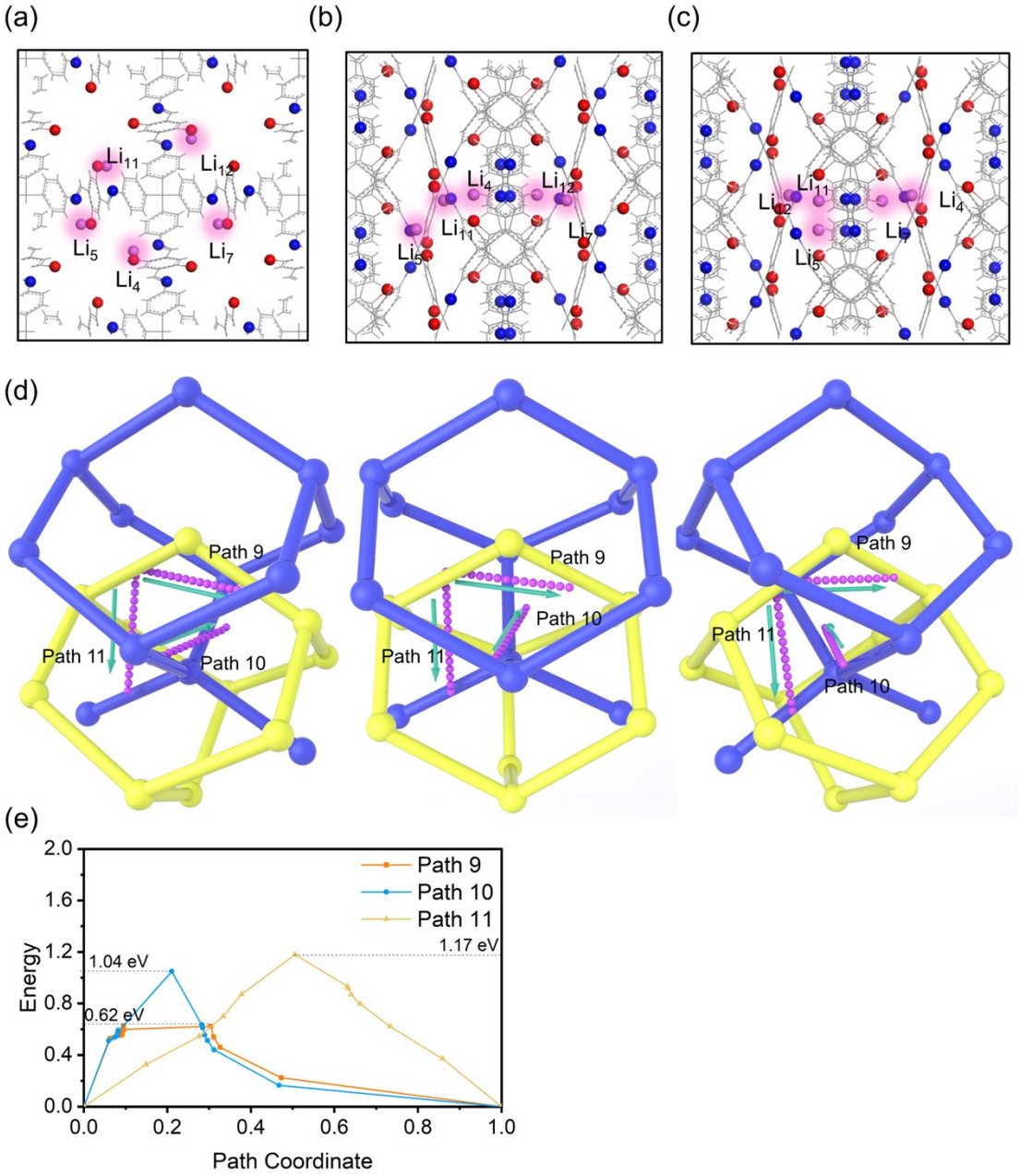

Fig. S15. Three views of Li^+ migration sites in TD-COF interlayer, top view (a) front view (b) and side view (c). Schematic representation of interlayer migration of Li^+ at different angles (d) and corresponding migration energy barriers (e).

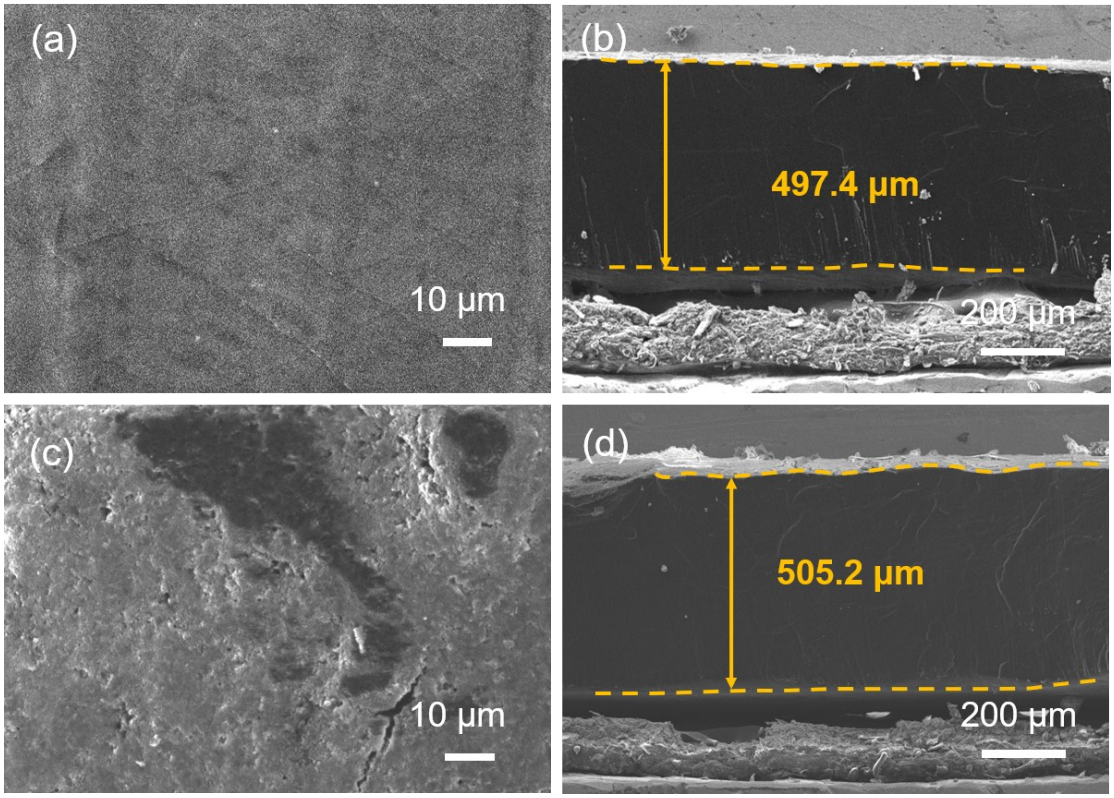

Fig. S16. SEM images of the bare Li (a-b) and TD-COF@Li (c-d) electrodes before cycling. Top view (a, d) and cross-section (b, d).

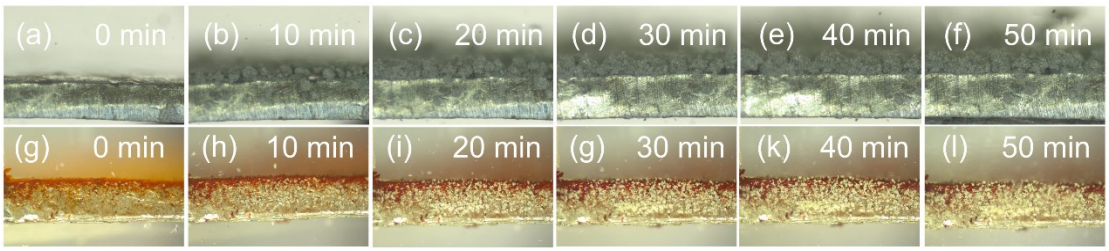

Fig. S17 In situ optical microscopy observation of Li deposition process on (a-f) bare Li and (g-l) TD-COF@Li at a current density of 5 mA cm^{-2} for 50min.

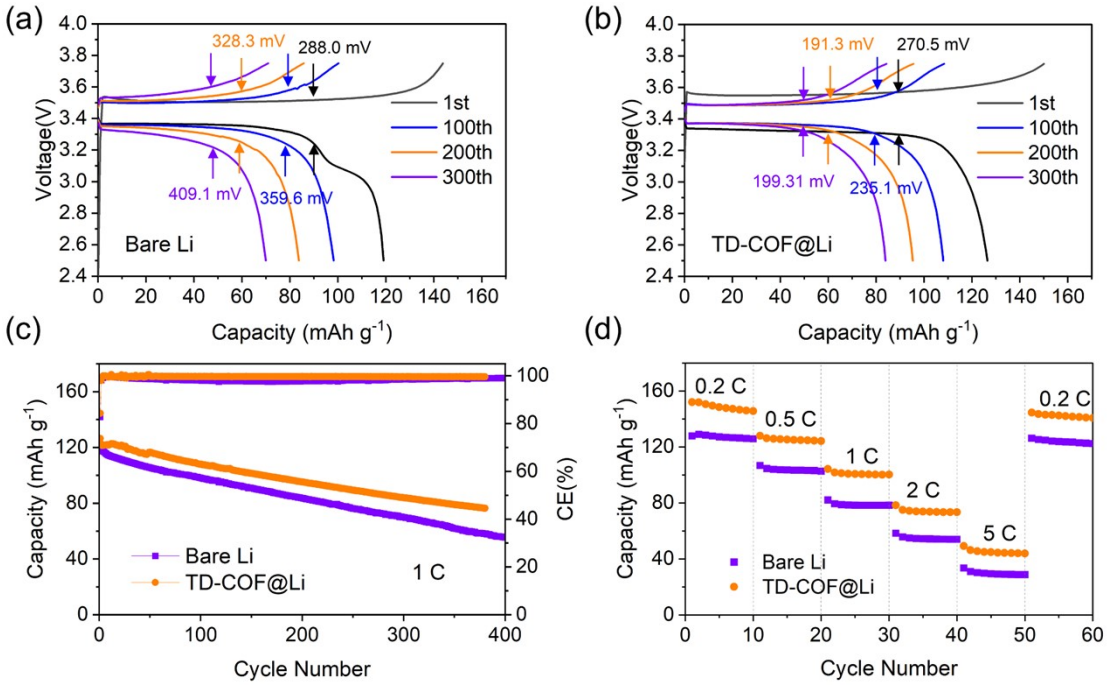

Fig. S18. Electrochemical performance of Li|LFP full batteries assembled with bare Li electrode and TD-COF@Li electrodes. The constant current charge/discharge profiles (a-b), long cycle performance at current of 1 C (c), and rate test operated ranging from 0.2 to 5 C (d).

References

[1] X.-J. Chen, C.-R. Zhang, X. Liu, J.-X. Qi, W. Jiang, S.-M. Yi, C.-P. Niu, Y.-J. Cai, R.-P. Liang and J.-D. Qiu, *Journal of Hazardous Materials*, 2023, **445**, 130442.

[2] R. D. Armstrong and H. Wang, *Electrochimica Acta*, 1994, **39(1)**,1-5.

[3] S. Zugmann, M. Fleischmann, M. Amereller, R. M. Gschwind, H. D. Wiemhöfer and H. J. Gores, *Electrochimica Acta*, 2011, **56**, 3926-3933.

[4] Z. Li, W. Ji, T.-X. Wang, Y. Zhang, Z. Li, X. Ding, B.-H. Han and W. Feng, *ACS Applied Materials & Interfaces*, 2021, **13**, 22586-22596.

[5] Z. Zhao, W. Chen, S. Impeng, M. Li, R. Wang, Y. Liu, L. Zhang, L. Dong, J. Unruangsri, C. Peng, C. Wang, S. Namuangruk, S.-Y. Lee, Y. Wang, H. Lu and J. Guo, *Journal of Materials Chemistry A*, 2020, **8**, 3459-3467.

[6] Y. Xu, Y. Zhou, T. Li, S. Jiang, X. Qian, Q. Yue and Y. Kang, *Energy Storage Materials*, 2020, **25**, 334-341.

[7] Y. Yang, C. Zhang, G. Zhao, Q. An, Z. y. Mei, Y. Sun, Q. Xu, X. Wang and H. Guo, *Advanced Energy Materials*, 2023, **13**, 2300725.

[8] H. Xie, Q. Hao, H. Jin, S. Xie, Z. Sun, Y. Ye, C. Zhang, D. Wang, H. Ji and L.-J. Wan, *Science China Chemistry*, 2020, **63**, 1306-1314.

[9] X. M. Lu, Y. Cao, Y. Sun, H. Wang, W. Sun, Y. Xu, Y. Wu, C. Yang and Y. Wang, *Angewandte Chemie International Edition*, 2024, **63**, e202320259.

[10] L. Yue, X. Wang, L. Chen, D. Shen, Z. Shao, H. Wu, S. Xiao, W. Liang, Y. Yu and Y. Li, *Energy & Environmental Science*, 2024, **17**, 1117-1131.

[11] C. Zhang, J. Xie, C. Zhao, Y. Yang, Q. An, Z. Mei, Q. Xu, Y. Ding, G. Zhao and H. Guo, *Advanced Materials*, 2023, **35**, 2304511.

[12] X. Wu, S. Zhang, X. Xu, F. Wen, H. Wang, H. Chen, X. Fan and N. Huang, *Angewandte Chemie International Edition*, 2024, **63**, e202319355.

[13] Y. Yang, C. Zhang, Z. Mei, Y. Sun, Q. An, Q. Jing, G. Zhao and H. Guo, *Nano Research*, 2023, **16**, 9289-9298.